Botong Li[1] / Deyi Liu[1] / Xuehui Chen[1] / Liancun Zheng[1]

Heat Transfer of Power-Law Liquid Food in a Tank with Varying Stirrer Settings

[1] School of Mathematics and Physics, University of Science and Technology Beijing, Beijing 100083, China, E-mail: libotong@ustb.edu.cn

Abstract:
In this article, we explore the heat transfer of non-Newtonian liquid food in the heating process in a channel connecting a tank. To achieve a rapid heat diffusion, several cylindrical agitators are inserted into the tank. We pay special attention to a Chinese traditional food, i.e. the black sesame paste, which is predicted by the power-law model. The fluid flow and heat transfer are investigated numerically, under the impacts of the angular velocity of cylinder, the stirrer size and the rotational direction. Three different settings are investigated: the two-stirrer, the three-stirrer, and the 2 × 2 stirrer settings. Several applicable strategies could be applied to improve the heat transfer in food engineering practices, including changing the size, the rotational velocity, the direction, and the number of stirrers in the heat exchanger.

Keywords: liquid food, power-law fluid, stirred tank

DOI: 10.1515/ijfe-2018-0282

Received: September 8, 2018; **Revised:** December 21, 2018; **Accepted:** March 7, 2019

1 Introduction

Liquid foods exist in the food industry, such as juice, honey, milk, cooking oil, and sugar pulp. Some of the solid food in molten state can also be regarded as fluid, such as chocolate. Under certain circumstances, many common liquid foods exhibit non-Newtonian characteristics, for example, mayonnaise is a kind of pseudo-plastic fluid; high-concentration sugar solution belongs to the plastic fluid; the chocolate pulp is similar to a typical Bingham plastic fluid; and the jelly is close to a certain viscoelastic fluid. The fluid that satisfies the linear relationship between shear stress and velocity gradient is called the Newton fluid, otherwise, when it does not satisfy the linearity relation, it is called a non-Newtonian fluid. Because the rheological properties of food have a vital influence on the food processing process, the investigations on the complex flow characteristics and physical mechanism of non-Newtonian fluid food is a topic of great concern for experts and scholars in recent years.

Many scholars have carried out the rheological properties of foods with their species, concentrations, temperatures, and different processing conditions. Fabbri *et al*. [1] got two kinds of food: Tara glue and dough, which were described by the non-Newtonian power-law fluid model. Anese *et al*. [2] used computational fluid dynamics to predict the viscosity distributions of tomato juice in different shape container by a modified power-law model. Kechichian *et al*. [3] set up a mathematical model to simulate the Chinese cabbage in the tubular system in the processing. The fruit was regarded as the pseudo-plastic non-Newtonian fluid, which was a kind of power-law fluid. Augusto *et al*. [4] studied the effects of the high pressure on the rheological properties of fruit juice, and the viscosity was found to decrease with the increasing pressure. Benkhelifa *et al*. [5] have designed a rheometer to study the rheological properties of the xanthan gum, which belonged to the power-law typed shear-thinning diluent. Song Yi *et al*. [6] studied the kinetic model of the supercritical fluid to describe the extraction of grape seed oil and almond oil. Yoshida *et al*. [7] developed a viscometer of a flow channel instrument which was easy to use to investigate both Newtonian and non-Newtonian typed liquid foods. Hassan *et al*. [8] studied the aqueous carboxymethyl cellulose solution with Nylon particles suspended in, and the liquid located in a rotary retort when fixed or free bi-axial rotation happened.

Inspired by above works, we investigate the non-Newtonian power-law model which can depict the rheological properties of many liquid food. The black sesame paste has been examined in our laboratory, which is proved to satisfy the power-law model. We will adopt it as a special case. The fluid flow and heat transfer of non-Newtonian fluids have already raised a great interest in the scientific field for its wide existence in various industrial processes. Some critical studies on the non-Newtonian fluids include, but not limited to, the follows: Assuming that the inner and outer ducts were held at different hot and cold temperature, Matin *et al*.

Botong Li is the corresponding author.

[9] investigated the two-dimensional steady-state non-Newtonian power-law fluid of natural convection between two horizontal square ducts numerically. By the multi-step differential transform method, Keimanesh *et al*. [10] investigated a third grade non-Newtonian fluid flowing through two parallel plates. Malvandi *et al*. [11] studied the static shear-thinning typed power-law fluids with spherical particles in it, and they solved the control equations by adopting the homotopy-perturbation method and the variational iteration technique. Galanis *et al*. [12] presented the solution for the hydrodynamically developed forced convection of power-law fluids, and its mass transfer happened with the phase change at the isothermal walls. Lin *et al*. [13] focused on the steady boundary layer of power-law fluids flowing through a flat with suction/injection and magnetic effects. Rashidi *et al*. [14] studied theoretically the boundary layers of the generalized third-grade viscoelastic power-law fluids. Khalili *et al*. [15] adopted the power-law fluid to configure nanofluids and presented the effects of both the Brownian motion and the thermophoresis on the nanofluid boundary layer over a stretching plate. Rashidi *et al*. [16] discussed the natural convection of incompressible non-Newtonian third-grade fluids flowing through two parallel surfaces. Eid *et al*. [17] also adopted the power-law fluid as the basefluids of nanofluids and addressed the combined effects of heat generation /absorption and the magnetic field on the boundary-layer of a nanofluid over a permeable stretching wall. Khan *et al*. [18] discussed the squirmy motion of non-Newtonian third-order fluids caused by asymmetric waves propagation on the walls of a channel which was inclined asymmetric. Besides, with nanofluids based power-law fluids, Bahiraei *et al*. [19] examined the irreversibilities caused by heat transfer and friction for nanofluids in a mini-channel which possessed chaotic perturbations. Lin *et al*. [20] presented a numerical investigation on the mass and heat transfer of Cu nanofluids with power-law base fluids in a circular groove with a relative slow revolution. Bhatti *et al*. [21] analyzed the entropy generation of the MHD non-Newtonian Williamson nanofluid over a porous shrinking surface.

A channel connecting a tank with several continuous stirrers are our configuration of interest. Liquid foods in up-to-date applications are always treated by means of stirring instead of primary and slow diffusion mechanism of fluid. For example, food is stirred in channels and tanks for preferable controllable delivery and rapid heat diffusion [22]. Islami *et al*. [22] studied the problem of a non-Newtonian nanofluid in two different cases: without and with micromixers. Both situations occur in a parallel plate microchannel with different nanoparticle loading parameters and varying Reynolds numbers. Alam *et al*. [23] studied a fluid in a microchannel numerically using three-dimensional Navier-Stokes equations. In our investigation, to achieve rapid heat diffusion and better sterilizing, a set of several cylindrical agitators are inserted into the tank improve the advection effect through stretching, roiling, folding and breaking of fluid flow. We study the forced laminar convection of power-law liquid fluid with heating boundary conditions. The results and figures reveal the influences of angular velocity of cylinder ω, stirrer size and direction, number of stirrers on the heat transfer and velocity field.

2 Problem description

2.1 Definition of geometry

The configuration of three geometries investigated in this research is shown in Figure 1. A channel connects a tank with several continuous stirrers in it. The width of the channel is L, while the one of the tank is H = 3 L. The channel is long enough to make sure that the fluid flow is fully developed when it comes into the tank. Uniform temperature is assumed at the inlet of the channel, while heaters are placed at the top and bottom walls of the tank. The adiabatic rotating cycloidal stirrers are all with a diameter of L. In our investigation, we will vary the numbers of the stirrers from two to four, and the rotation direction, speed and stirrer size on the velocities and temperature fields are revealed.

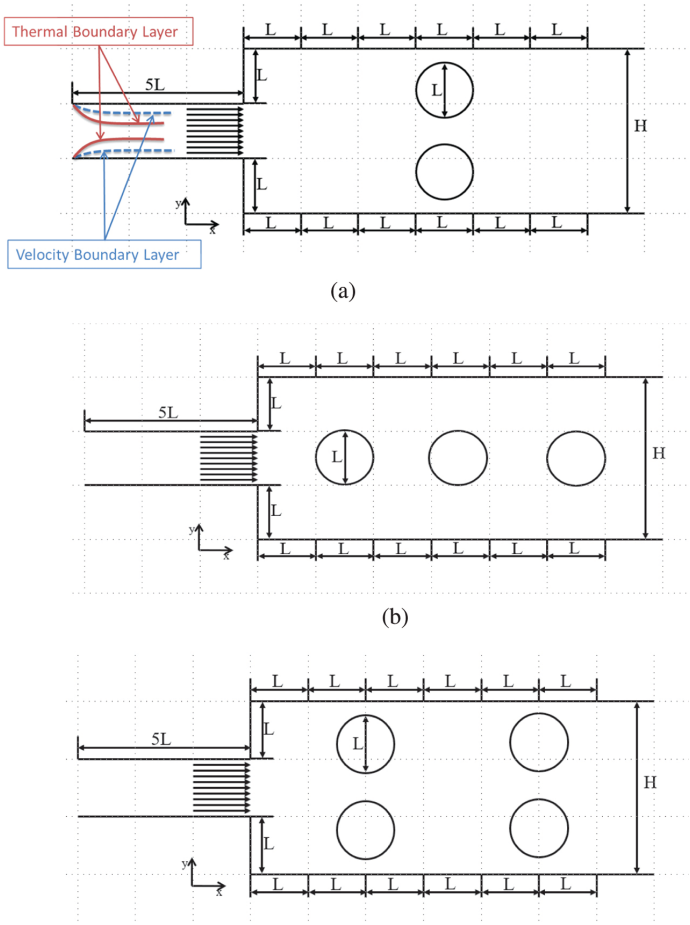

Figure 1: Nanofluids through the channel into the tank: (a) two stirrers in a line perpendicular to the flowing direction; (b) three stirrers in a line along the flowing direction; (c) 2 × 2 stirrers.

2.2 Governing equations

We investigate the two-dimensional incompressible steady state non-Newtonian power-law fluids in thermal equilibrium in the channel and the tank. The control equations are as follows:

Continuity:

$$\frac{\partial u}{\partial x} + \frac{\partial v}{\partial y} = 0 \tag{1}$$

Momentum:

$$\rho\left(u\frac{\partial u}{\partial x} + v\frac{\partial u}{\partial y}\right) = -\frac{\partial p}{\partial x} + \frac{\partial \tau_{xx}}{\partial x} + \frac{\partial \tau_{yx}}{\partial y} \tag{2}$$

$$\rho\left(u\frac{\partial v}{\partial x} + v\frac{\partial v}{\partial y}\right) = -\frac{\partial p}{\partial y} + \frac{\partial \tau_{xy}}{\partial x} + \frac{\partial \tau_{yy}}{\partial y} + g\rho\beta(T - T_0) \tag{3}$$

where

$$\tau_{xx} = 2\mu\left(2\left(\frac{\partial u}{\partial x}\right)^2 + 2\left(\frac{\partial v}{\partial y}\right)^2 + \left(\frac{\partial u}{\partial y} + \frac{\partial v}{\partial x}\right)^2\right)^{\frac{n-1}{2}}\frac{\partial u}{\partial x}$$

$$\tau_{yx} = \tau_{xy} = \mu\left(2\left(\frac{\partial u}{\partial x}\right)^2 + 2\left(\frac{\partial v}{\partial y}\right)^2 + \left(\frac{\partial u}{\partial y} + \frac{\partial v}{\partial x}\right)^2\right)^{\frac{n-1}{2}}\left(\frac{\partial u}{\partial y} + \frac{\partial v}{\partial x}\right)$$

$$\tau_{yy} = 2\mu\left(2\left(\frac{\partial u}{\partial x}\right)^2 + 2\left(\frac{\partial v}{\partial y}\right)^2 + \left(\frac{\partial u}{\partial y} + \frac{\partial v}{\partial x}\right)^2\right)^{\frac{n-1}{2}}\frac{\partial v}{\partial y}$$

In above equations, u presents the horizontal velocity and v the vertical velocity in the vector of $\mathbf{u} = (u, v)$; p represents the pressure. g is the gravity. For the physical characteristics of fluids, ρ is the density; β presents the thermal expansion coefficient; μ denotes the consistency index of power-law fluid; n is the power-law index. τ is the shear stress.

Energy:

$$\rho c_p\left(u\frac{\partial T}{\partial x} + v\frac{\partial T}{\partial y}\right) = \frac{\partial}{\partial x}\left(k\frac{\partial T}{\partial x}\right) + \frac{\partial}{\partial y}\left(k\frac{\partial T}{\partial y}\right) \tag{4}$$

where c_p is the fluid specific heat and T denotes the temperature. The parameter k is the thermal conductivity.

2.3 Non-dimensionalization and boundary conditions

To nondimensionalize the governing equations, x and y are scaled by L; u and v by U_0; the pressure p by $\frac{\mu {U_0}^n}{L^n}$; and T by T_0. Same symbols will be used in dimensionless equations for convenience.

$$\frac{\partial u}{\partial x} + \frac{\partial v}{\partial y} = 0 \tag{5}$$

$$\mathrm{Re}\left(u\frac{\partial u}{\partial x} + v\frac{\partial u}{\partial y}\right) = -\frac{\partial p}{\partial x} + \frac{\partial \tau_{xx}}{\partial x} + \frac{\partial \tau_{yx}}{\partial y} \tag{6}$$

$$\mathrm{Re}\left(u\frac{\partial v}{\partial x} + v\frac{\partial v}{\partial y}\right) = -\frac{\partial p}{\partial y} + \frac{\partial \tau_{xy}}{\partial x} + \frac{\partial \tau_{yy}}{\partial y} + \mathrm{Gr}(T-1) \tag{7}$$

$$\mathrm{Re}\cdot\mathrm{Pr}\left(u\frac{\partial T}{\partial x} + v\frac{\partial T}{\partial y}\right) = \frac{\partial^2 T}{\partial x^2} + \frac{\partial^2 T}{\partial y^2} \tag{8}$$

where

$$\tau_{xx} = 2\left(2\left(\frac{\partial u}{\partial x}\right)^2 + 2\left(\frac{\partial v}{\partial y}\right)^2 + \left(\frac{\partial u}{\partial y} + \frac{\partial v}{\partial x}\right)^2\right)^{\frac{n-1}{2}}\frac{\partial u}{\partial x}$$

$$\tau_{yx} = \tau_{xy} = \left(2\left(\frac{\partial u}{\partial x}\right)^2 + 2\left(\frac{\partial v}{\partial y}\right)^2 + \left(\frac{\partial u}{\partial y} + \frac{\partial v}{\partial x}\right)^2\right)^{\frac{n-1}{2}}\left(\frac{\partial u}{\partial y} + \frac{\partial v}{\partial x}\right)$$

$$\tau_{yy} = 2\left(2\left(\frac{\partial u}{\partial x}\right)^2 + 2\left(\frac{\partial v}{\partial y}\right)^2 + \left(\frac{\partial u}{\partial y} + \frac{\partial v}{\partial x}\right)^2\right)^{\frac{n-1}{2}}\frac{\partial v}{\partial y}$$

Additionally, $\mathrm{Re} = \rho L^n U_0^{2-n}/\mu$ is the generalized Reynolds number and $\mathrm{Pr} = c_p \mu L^{1-n}/k U_0^{1-n}$ is the generalized Prandtl number. $\mathrm{Gr} = T_0 L^{n+1} g\rho\beta/\mu U_0^n$ may be considered as the generalized Grashof number.

The non-dimensional boundary conditions are:

At the inlet: $u = 1, v = 0, T = 1$;

At the heating walls of the tank, i.e., top wall and bottom wall:

$$\frac{\partial T}{\partial y} = \begin{cases} -q_1, & \text{top wall} \\ -q_2, & \text{bottom wall} \end{cases}$$

At the outlet: $\frac{\partial u}{\partial x} = 0, \frac{\partial v}{\partial x} = 0$;
On the other walls: $u = 0, v = 0, \frac{\partial T}{\partial n} = 0$;
On the cylinder surface: $u = -\omega(y - y_0), v = \omega(x - x_0), \frac{\partial T}{\partial n} = 0$;

where q_i is the heat flux, ω denotes the cylinder angular velocity. A negative value of the velocity indicates clockwise rotation of the cylinder; while positive anti-clockwise rotation.

3 Numerical scheme

3.1 Weak formulation

Many researchers have applied various methods to calculate fluid flow and heat transfer problem, e.g. Li *et al.*'s work [24]. In the present research, the finite element method (FEM) with the aid of Freefem++ software is used in the calculation when a personal laptop possessing an Intel(R) Core(TM) i7-3520 CPU running at 4.00 GB of RAM and 2.90 GHz is used. The weak formulation is listed below:

The domain is defined as $\Omega \subset R^2$, and the boundary of Ω is Γ, which is sufficiently smooth (e.g., Lipschitz continuous). The velocity u and v is considered in space Z, defined as $H^1(\Omega)$ if $n \leq 1$ or $W^{1,n+1}(\Omega)$ if $n > 1$. The temperature T is in space W, defined as $W^{1,n+1}(\Omega)$ if $n > 3$ or $W^{1,4}(\Omega)$if $n \leq 3$. The pressure p is in $L^2(\Omega)$ (see Ref [25]). The weak formulation for eq.(5) is as [26]:

$$\int_\Omega \left(\left(\frac{\partial u}{\partial x} + \frac{\partial v}{\partial y} + \varepsilon p \right) q \right) d\mathbf{x} = 0, \forall q \in L^2(\Omega) \tag{9}$$

where ε is set to be $\varepsilon = 10^{-6}$ in the following computations. The weak formulations of eqs.(6–(8)) are:

$$\int_\Omega \left(\mathrm{Re} \left(\left(u \frac{\partial u}{\partial x} + v \frac{\partial u}{\partial y} \right) v_1 \right) - \frac{\partial v_1}{\partial x} p + \frac{\partial v_1}{\partial x} \tau_{xx} + \frac{\partial v_1}{\partial y} \tau_{yx} \right) d\mathbf{x} + \int_\Gamma p v_1 ds = 0, \ \forall v_1 \in Z \tag{10}$$

$$\begin{aligned} &\int_\Omega \left(\mathrm{Re} \left(\left(u \tfrac{\partial v}{\partial x} + v \tfrac{\partial v}{\partial y} \right) v_2 \right) - \tfrac{\partial v_2}{\partial y} p + \tfrac{\partial v_2}{\partial x} \tau_{xy} + \tfrac{\partial v_2}{\partial y} \tau_{yy} + \mathrm{Gr} \left((T-1) v_2 \right) \right) d\mathbf{x} \\ &- \int_\Gamma \left(2 (\tfrac{\partial u}{\partial x})^2 + 2 (\tfrac{\partial v}{\partial y})^2 + (\tfrac{\partial u}{\partial y} + \tfrac{\partial v}{\partial x})^2 \right)^{\frac{n-1}{2}} \tfrac{\partial u}{\partial y} v_2 ds = 0, \forall v_2 \in Z \end{aligned} \tag{11}$$

$$\begin{aligned} &\int_\Omega \left(\mathrm{Re} \cdot \mathrm{Pr} \left(\left(u \tfrac{\partial T}{\partial x} + v \tfrac{\partial T}{\partial y} \right) v_3 \right) + \tfrac{\partial T}{\partial x} \tfrac{\partial v_3}{\partial x} + \tfrac{\partial T}{\partial y} \tfrac{\partial v_3}{\partial y} \right) d\mathbf{x} \\ &+ \int_{\Gamma_1} q_1 v_3 ds + \int_{\Gamma_2} q_2 v_3 ds = 0, \forall v_3 \in Z \end{aligned} \tag{12}$$

where $\tau_{xx}, \tau_{xy}, \tau_{yx}, \tau_{yy}$ are defined as former.

3.2 Mesh and validation

The domain will be triangulated into a nonuniform triangular mesh. The triangular mesh we adopted in this research is illustrated in Figure 2.

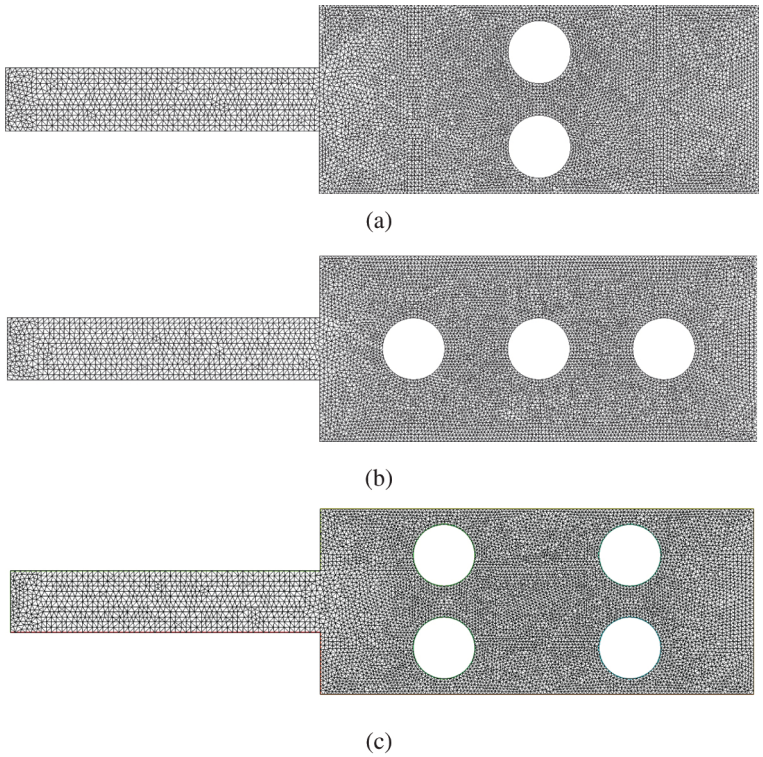

Figure 2: Triangular mesh: (a) two stirrers with 14,342 grids; (b) three stirrers with 14,430 grids; (c) 2 × 2 stirrers with 13,998 grids.

Continuous finite elements are used. Quadratic polynomial approximations in every element are employed for u, v and T, and a linear approximation is adopted for p. To handle the nonlinear terms, an iterative method is introduced into eqs.(9–(11)), i. e. the so-called 'ghost' time. $dt > 0$ is the time step size. $u^i = u(i \cdot dt, x, y)$, $v^i = v(i \cdot dt, x, y)$ and $T^i = T(i \cdot dt, x, y)$ are the information obtained at time i. The approximation solution at the next time step i can be calculated for the velocity at time step $i - 1$:

$$\int_\Omega \left(\left(\frac{\partial u^i}{\partial x} + \frac{\partial v^i}{\partial y} + \varepsilon p \right) q \right) d\mathbf{x} = 0, \forall q \in L^2(\Omega) \tag{13}$$

$$\begin{aligned} \int_\Omega \left(\frac{(u^i - u^{i-1})}{dt} v_1 + \mathrm{Re}\left(\left(u^{i-1} \frac{\partial u^{i-1}}{\partial x} + v^{i-1} \frac{\partial u^{i-1}}{\partial y} \right) v_1 \right) - \frac{\partial v_1}{\partial x} p + \frac{\partial v_1}{\partial x} \tau_{xx}^{i-1} + \frac{\partial v_1}{\partial y} \tau_{yx}^{i-1} \right) d\mathbf{x} \\ + \int_\Gamma p v_1 ds = 0, \forall v_1 \in Z \end{aligned} \tag{14}$$

$$\begin{aligned} \int_\Omega \left(\frac{(v^i - v^{i-1})}{dt} v_2 + \mathrm{Re}\left(\left(u^{i-1} \frac{\partial v^{i-1}}{\partial x} + v^{i-1} \frac{\partial v^{i-1}}{\partial y} \right) v_2 \right) - \frac{\partial v_2}{\partial y} p + \frac{\partial v_2}{\partial x} \tau_{xy}^{i-1} + \frac{\partial v_2}{\partial y} \tau_{yy}^{i-1} + \mathrm{Gr}\left((T^{i-1} - 1) v_2 \right) \right) d\mathbf{x} \\ - \int_\Gamma \left(2\left(\frac{\partial u^{i-1}}{\partial x}\right)^2 + 2\left(\frac{\partial v^{i-1}}{\partial y}\right)^2 + \left(\frac{\partial u^{i-1}}{\partial y} + \frac{\partial v^{i-1}}{\partial x}\right)^2 \right)^{\frac{n-1}{2}} \frac{\partial u^{i-1}}{\partial y} v_2 ds = 0, \forall v_2 \in Z \end{aligned} \tag{15}$$

The total time step can be regarded as the number of iterations. The continuity equations and the momentum equations can be first solved to obtain only the velocity and the pressure. By substituting both the velocity and the pressure into the temperature equation, the temperatures can be obtained. The iterative process stops as soon as the steady-state is obtained, and the velocity stops changing. The iterative solutions will definitely be an approximation of the steady-state equation solutions.

To validate the numerical method, the present technique has been adopted to calculate the velocity of similar work found in Selimefendigil *et al*. 's work [27]. They investigated the mixed convection of nanofluid in a channel with a backward facing step, which has also a rotating cylinder like ours inserted into it. The results obtained by the numerical method in present research are compared with solutions of a special case when $\frac{x}{H} = 8, \Omega =$

3, $\phi = 0.03$, Re $= 100$ (the same symbols are used here as in the literature [27]). In Figure 3, the line corresponds to results achieved by the method outlined in the present paper and the square symbol represents those obtained by other researchers. They agree well.

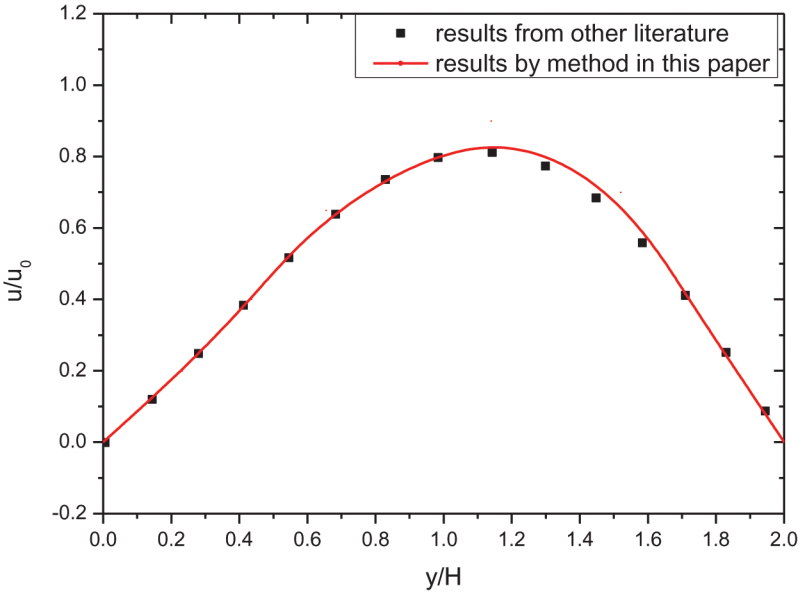

Figure 3: Results obtained by the method in present work in comparison with those from other literature [27].

4 Results and discussion

The current section presents primarily velocity field and temperature field calculated from FEM for different sets of stirrers with varying rotation direction, angular velocity, and stirrer size. We use parameters in the ranges as follows: for the power law index of fluids, $0.8 \leq n \leq 1.2$; for the stirrer radius, $0.4 \leq d \leq 0.6$; and for the cylinder angular velocity, $|\omega| \leq 4$.

4.1 Two-stirrer setting

In this section, we pay special attention on the effects of the rotational directions of the two stirrers on the fluid flow and temperature field. Figure 4 presents a brief and vivid comparison on the streamlines of the velocity fields with different rotation direction settings. The values of the rotational speed of both upper and lower stirrers are 4 in dimensionless form, when the rotational directions of the upper and lower stirrers keep the same or opposite.

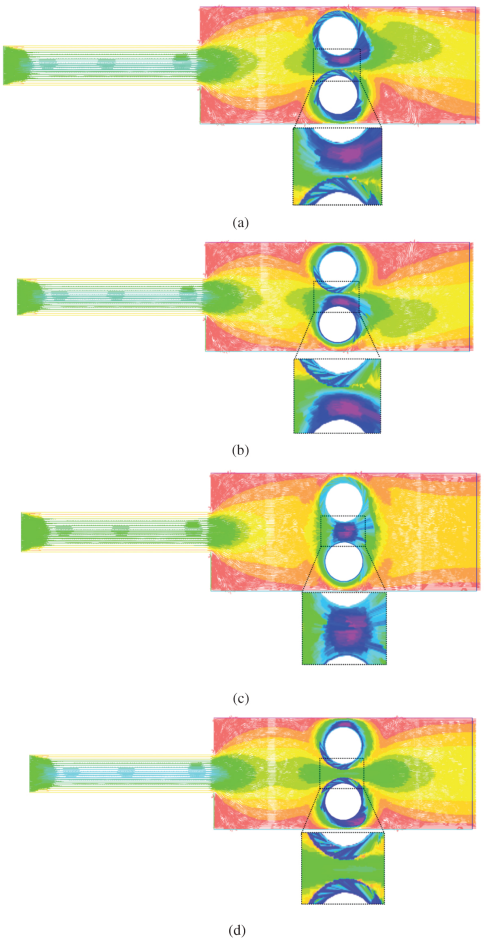

Figure 4: Velocity vectors for different rotational directions of two-stirrer setting when $\mathrm{Pr} = 1.0, \mathrm{Re} = 100, Gr = 0.1, n = 0.8, q_1 = q_2 = -1, |\omega| = 4$: (a)anti-clockwise(both); (b)clockwise(both); (c)anti-clockwise(upper), clockwise(lower) (d) clockwise(upper), anti-clockwise(lower).

Figure 5 reveals the temperatures on the bottom wall of the tank with different rotational directions of stirrers. We could find obvious peak and trough in these four curves which are the locations of the stirrers. From the figure, we can find an interesting phenomenon: the curve with square symbols is similar to the one with empty circle symbols; while the one with solid circle is similar to the one with triangles. It can be concluded that the rotational direction of the bottom stirrer decides the peak and trough of the temperature curve for thermal expansion exists. In engineering applications, changing the rotational directions of stirrers could change the peak and trough parts of temperature fields. It is also worth mentioning that regular residuals of curves in Figure 5(a) are depicted in Figure 5(b).

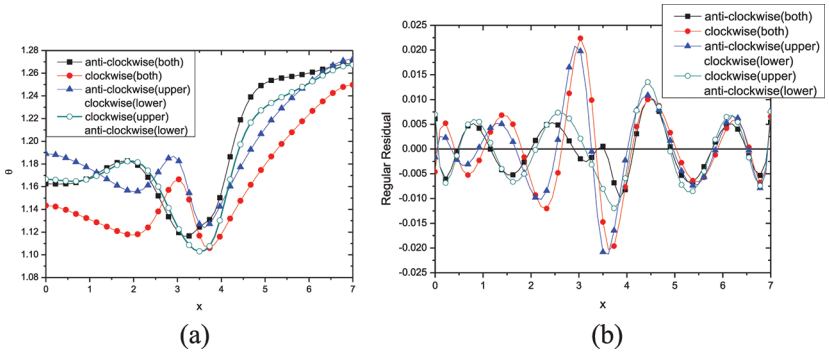

Figure 5: Temperature profiles along the tank walls at $y = -1.5$ for different rotational directions of two-stirrer setting when $\mathrm{Pr} = 1.0, \mathrm{Re} = 100, Gr = 0.1, n = 0.8, q_1 = q_2 = -1, |\omega| = 4$: (a) temperature distribution; (b) regular residuals of (a).

4.2 Three-stirrer setting

The isotherms in Figure 6 represent a brief comparison of the effects of varying rotational speeds on the temperature fields. From Figure 6, we can find out the temperature boundary layer are clear and alike in both cases, while the temperature isotherms around stirrers are totally different with varying rotational speed. The details of the differences of temperature fields are presented in 7. In Figure 7, we demonstrate the temperature of both the top ($y = 1.5$) and the bottom ($y = -1.5$) walls of the tank with $\mathrm{Pr} = 1.0, \mathrm{Re} = 100, Gr = 0.2, n = 1.2, q_1 = q_2 = -1$ for different angular velocities. With an increasing angular velocity, the temperatures on the top tank wall will increase while the temperatures on the bottom wall will fall. Thus, to increase the difference of temperature between top and bottom walls, we could speed up the rotational speed.

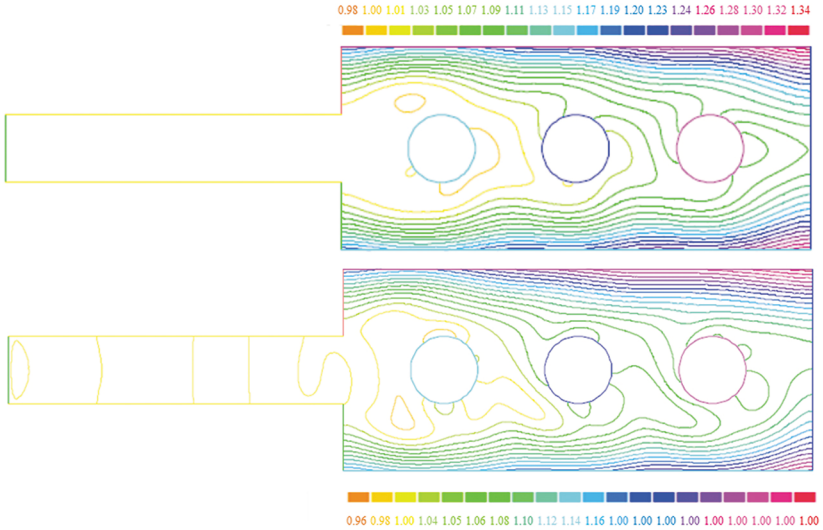

Figure 6: Isotherms for different rotational speeds of three anti-clockwise rotational stirrers when $\mathrm{Pr} = 1.0, \mathrm{Re} = 100, Gr = 0.2, n = 1.2, q_1 = q_2 = -1$: $\omega = 1$(top); $\omega = 3$(bottom).

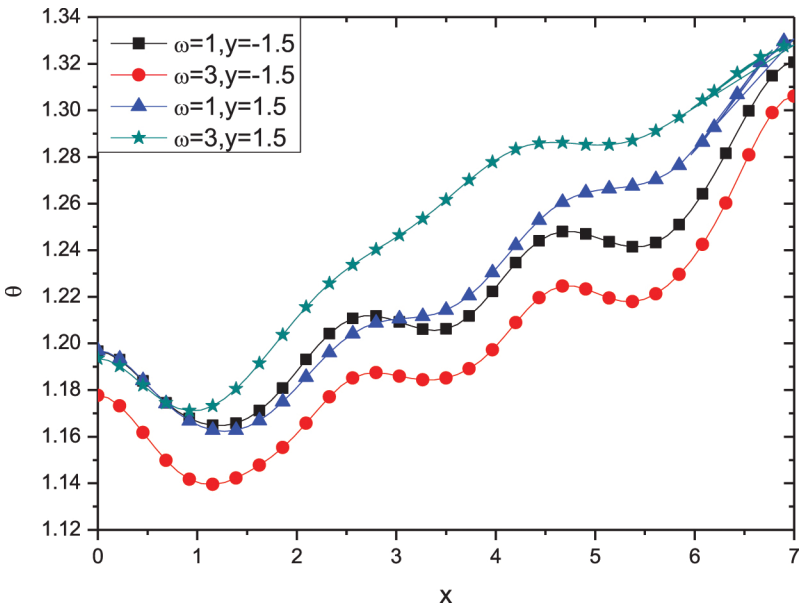

Figure 7: Temperature profiles along the top wall and the bottom wall for different rotational speeds of three anti-clockwise rotational stirrers when $\mathrm{Pr} = 1.0, \mathrm{Re} = 100, Gr = 0.2, n = 1.2, q_1 = q_2 = -1$.

4.3 Four-stirrer setting

In the above section, we keep the radius of the stirrer as $d = 0.5$ in dimensionless form. However, the stirrer size plays a very important part when the heat transfer of the tank is calculated, as illustrated in the following. Figure 8 reveals the size of the stirrer on the temperature profiles on the bottom walls. The values of the rotational velocity of all the four stirrers are 3 in dimensionless form. The rotational directions of the left stirrer on the top

line and the right stirrer on the bottom line are clockwise, while the others are anti-clockwise. An interesting phenomenon is observed: the temperature curve varies more intensely with a bigger stirrer. It looks like the temperature fields could be adjusted by changing the size of the stirrer only: the bigger the stirrer, the larger the amplitude of the temperature curves.

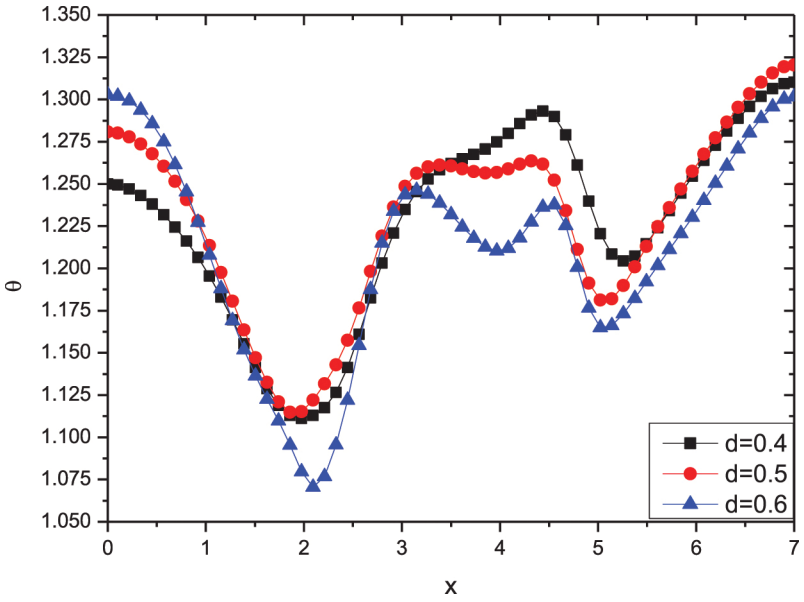

Figure 8: Temperature profiles along the bottom wall for different stirrer size of four stirrers when $\mathrm{Pr} = 1.0, \mathrm{Re} = 100, Gr = 0.3, y = -1.5, n = 0.8, q_1 = q_2 = -1, |\omega| = 3$.

4.4 Comparisons of different settings: a special case

In this section, we will compare the temperature fields and heat transfer of those three different stirrer settings above. For the food engineering reference, we choose a special Chinese traditional food, i.e. black sesame paste to investigate. Black sesame paste is a typical non-Newtonian power-law fluid with a power-law index of $n = 0.40178$, the rheology curve of which is measured by the Anton rheometer (MCR302) in our laboratory as Figure 9.

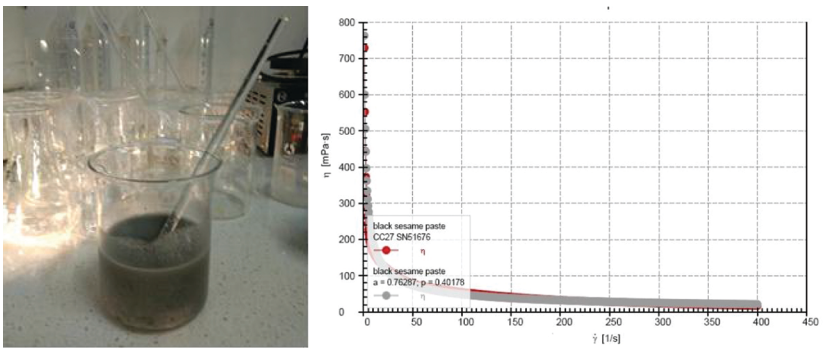

(a) (b)

Figure 9: (a) Black sesame paste; (b) rheology curve of Black sesame paste.

Figure 10 presents the temperature profiles of black sesame paste in a stirring tank with varying stirrer settings, but the stirrers of all settings are rotating anti-clockwise with speed of 1 in dimensionless form. From Figure 10, we can find out the temperature curves are complex with peak and trough in the position of stirrers. To evaluate the thermal performance of the tank with different stirrer settings better, we are going to compare the heat flux to the temperature differences. Average heat transfer coefficient are then calculated through the whole heating walls, i.e.

$$h_t = \frac{\int_{L_{top\ wall}} \frac{q_1}{(T_w(x)-T_0)} dx}{L_{top\ wall}}, \; h_b = \frac{\int_{L_{bottom\ wall}} \frac{q_2}{(T_w(x)-T_0)} dx}{L_{bottom\ wall}} \tag{16}$$

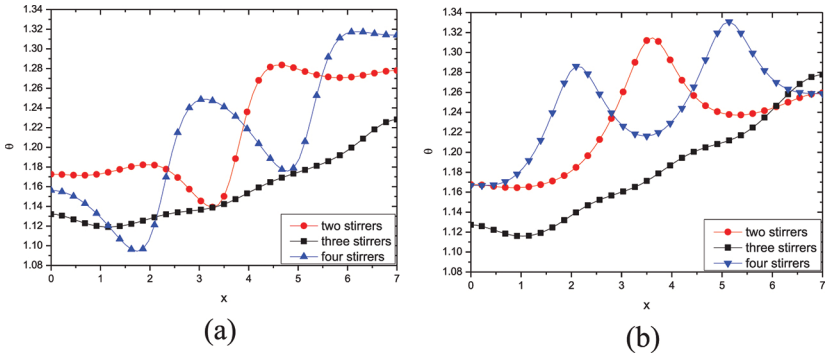

Figure 10: Temperature profiles of black sesame paste along the bottom wall(a) and top wall(b) for different settings of stirrers when $\mathrm{Pr} = 1.0, \mathrm{Re} = 100, Gr = 0.1, q_1 = q_2 = -1, \omega = 1$.

where $T_w(x)$ is the wall temperature at x.

The heat transfer coefficients of these three stirrer settings are listed in Table 1. From this Table, we can find out that the three-stirrer setting has the highest average heat transfer coefficient, even higher than the four-stirrer setting. Thus, to achieve a better heat transfer, it is recommendable to arrange all the stirrers in a line along the flowing direction, rather than put some stirrers in a line perpendicular to the flowing direction. Table 1 has also listed the CPU time we need when we adopt the numerical method mentioned in this paper to calculate the velocity and temperature fields of the channel and the tank with three different stirrer settings.

Table 1: Heat transfer coefficient and CPU time with different settings of stirrers.

Average heat transfer coefficient	Two-stirrer	Three-stirrer	Four-stirrer
Bottom wall	4.939	6.716	5.510
Top wall	4.603	6.058	4.233
CPU time (s)	393.3	442.9	416.9

5 Conclusions and future work

To investigate the heat transfer performance power-law typed liquid fluid flowing through a channel into a tank, different stirrer settings are adopted. The black sesame paste, a typical type of power-law fluid, is considered as an example. The influences of various parameters such as rotational direction, angular velocity of cylinderω, stirrer size and number on the heat transfer and velocity field are studied. Following results are obtained:

1. To achieve a better heat transfer, the three-stirrer setting in this investigation will be an efficient way.
2. The difference of temperature between top and bottom walls of the stirring tank will increase with a higher rotational velocity;
3. Changing the rotational directions of stirrers could change the peak and trough parts of temperature fields;
4. The temperature curve varies more intensely with a bigger stirrer;

Acknowledgements

The work of Botong Li is supported by the Fundamental Research Funds for the Central Universities (No. FRF-TP-17-020A1) and the National Natural Science Foundation of China (No.11402188), and Botong Li is very grateful to Mr Fengbin Sun for all his support and love.

Nomenclature

c_p fluid specific heat (J/kg · K)
d stirrer radius
Gr generalized Grashof number (Gr = $T_0 L^{n+1} g\rho\beta/\mu U_0^n$)
g gravity
h heat transfer coefficient (W/m^2 · K)
k thermal conductivity (W/m · K)
L length (m)
n power law index
Pr generalized Prandtl number (Pr = $c_p \mu L^{1-n}/kU_0^{1-n}$)
p pressure (Pa)
q_i heat flux (W/m^2)
Re Reynolds number (Re = $\rho L^n U_0^{2-n}/\mu$)
T temperature (K)
u, v velocities along x and y, respectively (m/s)
x, y Cartesian coordinates along the wall and normal to the wall, respectively (m)

Greek symbols

Ω calculation domain
Γ boundary of Ω
β thermal expansion coefficient
ρ fluid density (kg/m^3)
ω cylinder angular velocity
τ shear stress
μ consistency index(Pa · s^n)

Subscripts

t top wall
b bottom wall
0 inlet condition

References

[1] Fabbri A, Cevoli C. Rheological parameters estimation of non-Newtonian food fluids by finite elements model inversion. J Food Eng. 2016;169:172–8.
[2] Anese A, Bonis MVD, Mirolo G, Ruocco G. Effect of low frequency, high power pool ultrasonics on viscosity of fluid food: modeling and experimental validation. J Food Eng. 2013;119:627–32.
[3] Kechichian V, Crivellari GP, Gut JAW, Tadini CC. Modeling of continuous thermal processing of a non-Newtonian liquid food under diffusive laminar flow in a tubular system. Int J Heat Mass Tran. 2012;55:5783–92.
[4] Augusto PED, Ibarz A, Cristianini M. Effect of high pressure homogenization (HPH) on the rheological properties of a fruit juice serum model. J Food Eng. 2012;111:474–7.
[5] Benkhelifa H, Alvarez G, Flick D. Development of a scraper-rheometer for food applications: rheological calibration. J Food Eng. 2008;85:426–34.
[6] Song Y, Zheng LC, Zhang XX. Kinetics model for supercritical fluid extraction with variable mass transport. Int J Heat Mass Tran. 2017;112:876–81.
[7] Yoshida M, Igarashi H, Iwasaki K, Fuse S, Tsuruta Y, Shimomura T. Flow analysis for a flow channel instrument to evaluate viscosities of non-Newtonian viscoelastic liquid foods. I J Food Eng. 2017;13:20160403.
[8] Hassan HF, Ramaswamy HS, Dwivedi M. Overall and fluid-to-particle heat transfer coefficients associated with canned particulate non-Newtonian fluids during free bi-axial rotary thermal processing. Int J Food Eng. 2012;8. DOI: 10.1515/1556-3758.2392.
[9] Matin MH, Pop I, Khanchezar S. Natural convection of power-law fluid between two-square eccentric duct annuli. J Non-Newtonian Fluid Mech. 2013;197:11–23.

[10] Keimanesh M, Rashidi MM, Chamkha AJ, Jafari R. Study of a third grade non-Newtonian fluid flow between two parallel plates using the multi-step differential transform method. Comput Math Appl. 2011;62:2871–91.
[11] Malvandi A, Moshizi SA, Ganji DD. An analytical study on unsteady motion of vertically falling spherical particles in quiescent power-law shear-thinning fluids. J Mol Liq. 2014;193:166–73.
[12] Galanis N, Rashidi MM. Entropy generation in non-Newtonian fluids due to heat and mass transfer in the entrance region of ducts. Heat Mass Tran. 2012;48:1647–62.
[13] Lin YH, Zheng LC, Li BT, Ma LX. A new diffusion for laminar boundary layer flow of power law fluids past a flat surface with magnetic effect and suction or injection. Int J Heat Mass Tran. 2015;90:1090–7.
[14] Rashidi MM, Rastegari MT, Asadi M, Bég OA. A study of non-Newtonian flow and heat transfer over a non-isothermal wedge using the homotopy analysis method. Chem Eng Commun. 2012;199:231–56.
[15] Khalili S, Tamim H, Khalili A, Rashidi MM. Unsteady convective heat and mass transfer in pseudoplastic nanofluid over a stretching wall. Adv Powder Technol. 2015;26:1319–26.
[16] Rashidi MM, Hayat T, Keimanesh M, Hendi AA. New analytical method for the study of natural convection flow of a non-Newtonian fluid. Int J Numer Method H. 2013;23:436–50.
[17] Eid MR, Mahny KL. Unsteady MHD heat and mass transfer of a non-Newtonian nanofluid flow of a two-phase model over a permeable stretching wall with heat generation/absorption. Adv Powder Technol. 2017;28:3063–73.
[18] Khan AA, Sohail A, Rashid S, Rashidi MM, Khan NA. Effects of slip condition, variable viscosity and inclined magnetic field on the peristaltic motion of a non-Newtonian fluid in an inclined asymmetric channel. J Appl Fluid Mech. 2016;9:1381–93.
[19] Bahiraei M, Gharagozloo K, Alighardashi M, Mazaheri N. CFD simulation of irreversibilities for laminar flow of a power-law nanofluid within a minichannel with chaotic perturbations: an innovative energy-efficient approach. Energ Convers Manage. 2017;144:374–87.
[20] Lin YH, Jiang YY. Effects of Brownian motion and thermophoresis on nanofluids in a rotating circular groove: A numerical simulation. Int J Heat Mass Tran. 2018;123:569–82.
[21] Bhatti MM, Abbas T, Rashidi MM. Numerical study of entropy generation with nonlinear thermal radiation on magnetohydrodynamics non-Newtonian nanofluid through a porous shrinking sheet. J Magn. 2016;21:468–75.
[22] Islami SB, Dastvareh B, Gharraei R. An investigation on the hydrodynamic and heat transfer of nanofluid flow, with non-Newtonian base fluid, in micromixers. Int J Heat Mass Tran. 2014;78:917–29.
[23] Alam A, Kim K-Y. Analysis of mixing in a curved microchannel with rectangular grooves. Chem Eng J. 2012;181–2:708–16.
[24] Li F. Backward solutions to Neumann and Dirichlet problems of heat conduction equation. Appl Math Comput. 2009;210:211–14.
[25] Shi HD, Lin P, Li BT, Zheng LC. A finite element method for heat transfer of power-law flow in channels with a transverse magnetic field. Math Method Appl Sci. 2014;37:1121–9.
[26] Lin P, Liu C. Simulations of singularity dynamics in liquid crystal flows: A Co finite element approach. J Comput Phys. 2006;215:348–62.
[27] Selimefendigil F, Öztop HF. Numerical investigation and reduced order model of mixed convection at a backward facing step with a rotating cylinder subjected to nanofluid. Comput Fluids. 2015;109:27–37.